

Quantum Phase Transitions of Trilayer Excitons in Atomically Thin Heterostructures

Yevgeny Slobodkin,¹ Yotam Mazuz-Harpaz¹,¹ Sivan Refaely-Abramson,² Snir Gazit^{1,3},
Hadar Steinberg¹,¹ and Ronen Rapaport^{1,*}

¹The Racah Institute of Physics, The Hebrew University of Jerusalem, Jerusalem 9190401, Israel

²Department of Materials and Interfaces, Weizmann Institute of Science, Rehovot 7610001, Israel

³The Fritz Haber Research Center for Molecular Dynamics, The Hebrew University of Jerusalem, Jerusalem 9190401, Israel



(Received 22 April 2020; accepted 17 November 2020; published 18 December 2020)

We determine the phase diagram of excitons in a symmetric transition-metal dichalcogenide 3-layer heterostructure. First principles calculations reveal interlayer exciton states of a symmetric quadrupole, from which higher energy asymmetric dipole states are composed. We find quantum phase transitions between a repulsive quadrupolar and an attractive staggered dipolar lattice phases, driven by a competition between interactions and single exciton energies. The different internal quantum state of excitons in each phase is a striking example of a system where single-particle and interacting many-body states are coupled.

DOI: 10.1103/PhysRevLett.125.255301

Introduction.—The quantum ground state of many-body systems is determined by a nontrivial interplay between interparticle interactions and the delocalization induced by the kinetic energy. When interactions between particles are extended in space (e.g., in the case of dipolar particles), the many-body system may display significant particle correlations [1–3]. These many-body correlations can lead to exotic effects such as Roton instabilities [4] and super-solidity, both recently observed in ultracold gases of dipolar atoms [5–10]. In semiconductor quasiparticle systems, collective correlated phases of interacting dipolar excitons in 2D heterostructures were observed, first in GaAs bilayers [11–16], and more recently in van der Waals (vdW) heterostructures [17,18].

Quite generally, the form of interaction is encoded in the intrinsic properties of the elementary constituents determined by the internal structure, hence the interaction remains a static property. In typical realizations of dipolar atoms or excitons, the size and orientation of the dipole moment are fixed and set by an external field (magnetic or electric). Specifically for spatially indirect (interlayer) excitons, which are quasiparticles formed by binding of excited electrons and holes residing in adjacent layers, the magnitude and orientation of the dipole moment are determined by the structural composition. This in turn dictates the exciton-exciton interactions. In this regard, heterostructure systems have an intrinsic decoupling between the single particle state and the collective state of many particles.

In this Letter, we study theoretically excitons in a transition-metal dichalcogenide (TMD) trilayer heterostructure, and find a new phenomenon of coupling between internal particle properties and the many-body state, making the single particle structure and the particle-particle interaction dynamical parameters rather than static ones. We show that this unique situation gives rise to a quantum phase transition

between two symmetry distinct phases, each made of completely different elementary exciton quasiparticles: a nonpolar, weakly interacting many-body state at lower particle densities, a staggered dipolar state with strong interactions at higher densities, and a phase instability leading to a droplet phase.

Single quadrupolar and dipolar excitons.—TMD heterostructures composed of stacked TMD monolayers have been shown to host long-lived excitons, a consequence of suppressed overlap between the wave functions in separate layers [19–28]. A commonly explored heterojunction is a bilayer composed of WSe₂ and MoSe₂ monolayers, where the conduction electrons and valence holes are localized at separate layers, resulting in interlayer excitons with a fixed, oriented electric dipole moment [29–35]. Here we consider a trilayer stack, obtained by adding a second WSe₂ layer—forming the WSe₂/MoSe₂/WSe₂ structure depicted in Fig. 1(e). Trilayer stacks, studied in photoluminescence [36,37], show indications of shortened exciton lifetime due to the enhanced wave-function overlap between the electron, which resides at the central MoSe₂ layer, and the hole, which is symmetrically delocalized between the two WSe₂ layers [37]. The interplay between such a hole-delocalized, quadrupolar exciton and the bilayer dipolar excitons results in a rich many-body phase diagram.

To find the lowest lying exciton states, we start by computing the single particle band structure using a many-body perturbation theory within the GW and Bethe-Salpeter equation (GW-BSE) approximation [38–40]. The full computational details are given in Ref. [41]. Figure 1(a) shows the quasiparticle band structure of the trilayer system. Notably, the valence *K* valley is split into upper and lower bands. The upper (with energy E_h^+) corresponds to the *z*-symmetric hole state ψ_h^+ , which includes significant hole distribution on the MoSe₂

layer. The lower (with energy E_h^-) corresponds to the z -antisymmetric hole state ψ_h^- , where these contributions are absent [Fig. 1(b)]. The energy split between the two bands at the K point (shown in the inset), $\Delta^\pm = E_h^+ - E_h^-$, is analogous to that of the bonding and antibonding orbitals in a double-well system [see blue and red cross sections in Fig. 1(d)]. As Δ^\pm depends on the interlayer distance d , we allow for possible variation in d , yielding $\Delta^\pm = 20$ –60 meV (see Supplemental Material [41]). We note that the valence band split is not due to spin-orbit interactions, and exists in both spin channels.

An interlayer exciton is formed by, e.g., a direct optical excitation of an electron from the valence to conduction band at the K valley. We assume that the timescale for scattering into other valleys is long, and focus on K -valley processes alone. The lowest lying single exciton bound state, denoted ψ_X^+ , with excitation energy $E_X^+ = 1.05$ eV [Fig. 1(c)], is composed of a K -valley conduction electron state, ψ_e , spatially localized in the central MoSe₂ layer, and a K -valley valence hole state, ψ_h^+ , with a wave function delocalized in the z direction between the symmetric top and bottom layers (see Ref. [41]). The second exciton state, ψ_X^- , with excitation energy $E_X^- = 1.1$ eV, is composed of ψ_e and ψ_h^- . Contrary to the bilayer exciton picture, ψ_X^\pm have a zero dipole and a finite quadrupole moment [shown schematically in Fig. 1(e), left] and are therefore named quadrupolar excitons. The exciton binding energies of the two quadrupolar states are given by $E_b^\pm = E_e + E_h^\pm - E_X^\pm$. Our calculation shows that the binding energies E_b^+ and E_b^- , for the symmetric and antisymmetric quadrupole excitons, respectively, are almost identical (0.36 and 0.35 eV). The difference

between the energies of two quadrupolar excitons is therefore very close to the valence band split, $E_X^+ - E_X^- \approx \Delta^\pm$.

We now turn to the construction of the K -valley dipolar states, ψ_X^u and ψ_X^d , as in a double-well model, as shown in Fig. 1(d). To do that, we construct hole states localized in the top (bottom) layer, $\psi_h^{u(d)}$, by adding and subtracting the two delocalized hole states: $|\psi_h^{u(d)}\rangle = (1/\sqrt{2})(|\psi_h^+\rangle \pm |\psi_h^-\rangle)$ (where we assume opposite phases at the different WSe₂ layers in ψ_h^-), with energies $E_h^u = E_h^d = \frac{1}{2}(E_h^+ + E_h^-)$. The dipolar exciton states $\psi_X^{u(d)}$ are then constructed by an electron state ψ_e and a hole state $\psi_h^{u(d)}$, localized in the upper (lower) layer: $|\psi_X^{u(d)}\rangle = (1/\sqrt{2})(|\psi_X^+\rangle \pm |\psi_X^-\rangle)$. These excitons, depicted on the right side of Fig. 1(e) have a nonvanishing electric dipole moment, each pointing in an opposite direction. Since $E_b^+ \approx E_b^-$, and the dipolar excitons are linear superpositions of the quadrupolar excitons, the binding energies of the two types of dipolar excitons, $E_b^{u(d)}$, are approximately equal to those of the quadrupolar excitons. Thus the energy of both dipolar exciton states is given by $E_X^{u(d)} = E_e + E_h^{u(d)} - E_b^{u(d)} \approx E_e + E_h^{u(d)} - E_b^\pm$. The energy gap between the hole-symmetric quadrupolar exciton and the dipolar excitons, Δ_{DQ} , can therefore be evaluated to be

$$\Delta_{DQ} = E_X^{u(d)} - E_X^+ \approx E_h^{u(d)} - E_{h,+} = \Delta^\pm/2, \quad (1)$$

which yields $\Delta_{DQ} = 10$ –30 meV for the above layered structure. In what follows, we will show that Δ_{DQ} is an important parameter affecting the possible ground

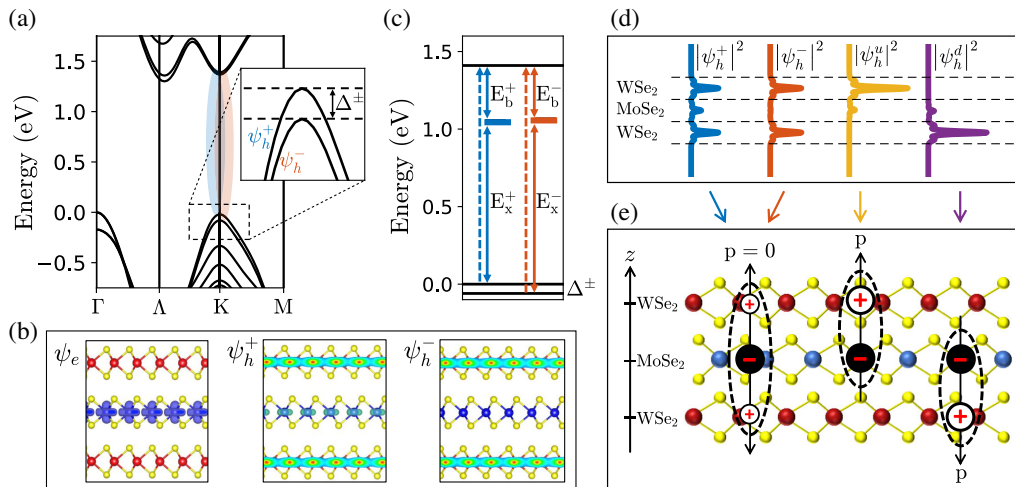


FIG. 1. (a) Calculated GW quasiparticle band structure of the WSe₂/MoSe₂/WSe₂ heterostructure. The inset shows the valence energy split at the K region (Δ^\pm). (b) Quasiparticle wave functions of the two split valence bands at K , and the corresponding schematic representation of a double-well symmetric and antisymmetric wave functions. (c) Exciton transition energies diagram for the two low lying excitons with energies E_X^+ and E_X^- , composed of $v \rightarrow c$ and $v - 1 \rightarrow c$ transitions, with binding energies E_b^+ and E_b^- , respectively. (d) Spatial cross section along the z direction of the probability density of the hole wave function in the quadrupolar ($|\psi_h^{+(-)}|^2$) and dipolar exciton states ($|\psi_h^{u(d)}|^2$). (e) Schematic illustration of dipolar ($p||z$, $p||-z$) and quadrupolar ($p = 0$) exciton states.

states in the many-exciton limit. Since $E_X^+ < E_X^{u(d)} < E_X^-$, in the following we only focus on the lowest energy hole-symmetric quadrupole exciton ψ_X^+ , and the two degenerate dipolar excitons $\psi_X^{u(d)}$.

Finite density of excitons: Phase transitions at $T = 0$.— With the quadrupolar and dipolar single exciton states established, we now turn to discuss the many-body phase diagram at finite exciton density, n .

In constructing our effective low-energy description, we consider only the dilute exciton limit, where the typical interexciton distance is significantly larger than the exciton size (set by the electron-hole bound state). This allows us to treat excitons as pointlike bosonic quasiparticles and safely neglect corrections arising due to fermionic exchange [16]. The two dipolar states $\psi_X^{u,d}$ can be conveniently parametrized by an Ising degree of freedom $|\sigma^z = u, d\rangle$. The exciton dynamics is governed by the Hamiltonian (setting $\hbar = 1$),

$$\mathcal{H} = -\frac{1}{2m_x} \sum_i \nabla_i^2 + \sum_{i < j} V_{\sigma_i^z, \sigma_j^z}^d (|r_j - r_i|) - \Delta_{DQ} \sum_i \sigma_i^x. \quad (2)$$

In the above equation, i labels excitons and m_x denotes the effective in-plane exciton mass. The layer dependent dipolar interaction reads

$$\begin{aligned} V_{\sigma_i^z, \sigma_j^z}^d(r) &= V_{p,p}(r) \delta_{\sigma_i^z, \sigma_j^z} + V_{p,-p}(r) \delta_{\sigma_i^z, -\sigma_j^z}, \\ V_{p,p}(r) &= \frac{e^2}{\kappa} \left(\frac{2}{r} - \frac{2}{\sqrt{r^2 + d^2}} \right), \\ V_{p,-p}(r) &= \frac{e^2}{\kappa} \left(\frac{1}{r} + \frac{1}{\sqrt{r^2 + (2d)^2}} - \frac{2}{\sqrt{r^2 + d^2}} \right). \end{aligned} \quad (3)$$

Here, $V_{p,p}$ and $V_{p,-p}$ denotes the electrostatic energy associated with a parallel $[(u, u)$ or $(d, d)]$ and antiparallel $[(u, d)$ or $(d, u)]$ configuration of two dipolar excitons. d is the interlayer distance and κ is the effective dielectric constant, taken from our GW calculation as the dielectric function at the interaction distance corresponding to the interlayer separation [41]. The operator $\sigma^x|u\rangle = |d\rangle$, $\sigma^x|d\rangle = |u\rangle$ locally flips the dipole moment orientation. We note that the Hamiltonian affords a \mathbb{Z}_2 Ising symmetry corresponding to a global flip of the dipole moment orientation $\sigma_i^z \rightarrow -\sigma_i^z$ for all i .

To highlight the interplay between dipolar and quadrupolar states, we quench the in-plane exciton dynamics, namely, $e^2 \sqrt{n}/\kappa m_x \ll 1$. In this limit, the ground state is determined by a competition between the electrostatic energy and the quantum dynamics of the dipole orientation, as described by the second and third terms in Eq. (2), respectively.

The typical scale of the potential energy term of the Hamiltonian is $e^2/\kappa d$, and of the quantum dynamics is Δ_{DQ} , suggesting a dimensionless parameter as their ratio:

$R = \Delta_{DQ} \kappa d / e^2$. The zero-temperature ground state of the many particle system is determined in a two-parameter phase diagram controlled by R and n . To gain insight into the possible competing phases, we begin by establishing the ground state configuration in the various parameter limits, and then analyze the boundaries between these phases.

First, we consider the limiting case $R \rightarrow \infty$ for any finite density n . In this case the last term in Eq. (2) dominates. Consequently, strong quantum fluctuations in the dipole moment orientation favor a fully quadrupolar ground state, $|\psi_X^+\rangle = |+\rangle = (1/\sqrt{2})(|u\rangle + |d\rangle)$. Since quadrupolar electrostatic interactions, $(+) \leftrightarrow (+)$, are purely *repulsive*, minimizing the electrostatic energy leads to a triangular lattice structure [41] with broken translational symmetry; see left panels of Fig. 2(d). In Fig. 2(a) we plot the total

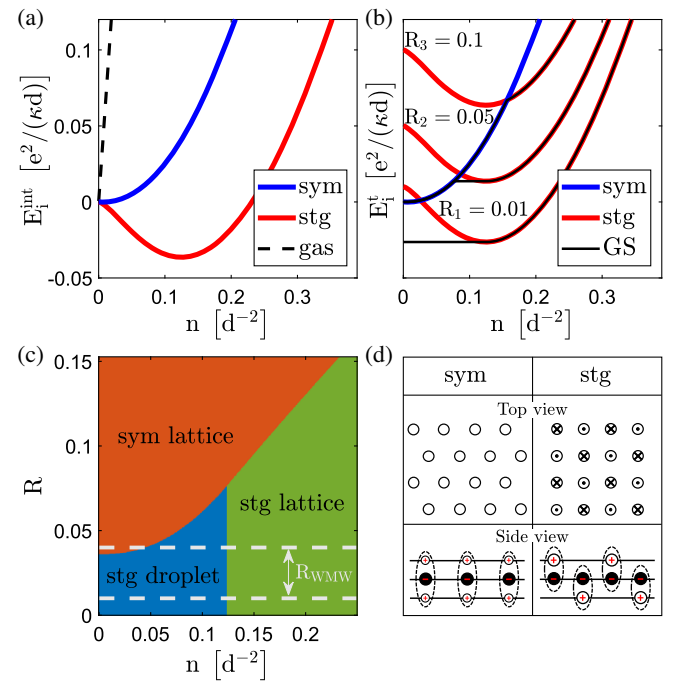


FIG. 2. (a) Electrostatic interaction energy E_i^{int} vs the density of excitons n . stg represents a staggered square lattice of dipolar excitons, where nearest neighbors have antiparallel dipole moments. sym represents a triangular lattice of quadrupolar excitons. The minimum energy (stg) appears at $n_d \approx 0.12 d^{-2}$. Dashed black represents an uncorrelated exciton gas (see Ref. [41]). (b) Total energy per particle E_i^t (where $i = \text{sym/stg}$) vs the density of excitons n . GS represents the many body ground state (black lines). Three different phase transitions are displayed: stg droplet \rightarrow stg lattice ($R_1 = 0.01$), sym lattice \rightarrow stg droplet \rightarrow stg lattice ($R_2 = 0.05$), sym lattice \rightarrow stg lattice ($R_3 = 0.1$). (c) Phase diagram. R represents the ratio of the energy difference between a dipolar and a quadrupolar single exciton state and the potential energy scale $e^2/\kappa d$. Dashed gray lines represent the upper and lower estimates for R_{WMW} , the special case of a $\text{WSe}_2/\text{MoSe}_2/\text{WSe}_2$ trilayer. (d) Schematic illustration of the competing phases in a three-layer structure with dipolar and quadrupolar excitons.

electrostatic energy per exciton, $E_{\text{sym}}^{\text{int}}(n)$ in the above configuration. It is simple to show that it rises as $E_{\text{sym}}^{\text{int}} \sim n^{5/2}$ at low density, $nd^2 \ll 1$ (Supplemental Material [41]).

Next, we examine the high density $nd^2 \rightarrow \infty$ limit for finite R , for which the electrostatic energy contribution in Eq. (2) overwhelms all other terms and hence should be minimized. A key observation is that in contrast to quadrupoles which always repel, antiparallel dipoles, $(u) \leftrightarrow (d)$, attract at long distances leading to an electrostatic energy gain at all densities compared to the symmetric case, as is seen in Fig. 2(a). Therefore at this limit, the system favors a competing dipolar configuration comprising a staggered pattern of dipole orientations; see the right panels of Fig. 2(d). The particular choice of a square lattice (as opposed to a triangular lattice, see Supplemental Material [41]) allows avoiding the inherent frustration of staggered configurations on nonbipartite lattices [56]. Importantly, the staggered state not only breaks translational symmetry, but also the Ising layer symmetry. The total electrostatic energy per exciton of the staggered state, $E_{\text{stg}}^{\text{int}}(n)$, evolves nontrivially as a function of density, see Fig. 2(a). At low densities, the energy turns negative, $E_{\text{stg}}^{\text{int}}(n) \sim -n^{3/2}$. However, with increasing n , the interaction energy increases and turns positive, due to the short range repulsive interaction. The energy minimum is obtained at $n_d \approx 0.12d^{-2}$, at which the interaction energy equals $E_{\text{stg}}^{\text{int}}(n_d) \approx -0.036e^2/(\kappa d)$.

Next, we turn to determine the phase boundaries separating the staggered dipolar and layer-symmetric quadrupolar states. To that end, we examine the total energy per exciton $E^i = E_X + E^{\text{int}}(n)$, and compare the total energies in the two competing states: E_{sym}^i vs E_{stg}^i . Clearly, this variational approach is approximate, as it neglects quantum fluctuations. We leave the question of determining their role to a future study (see a discussion on zero-point fluctuations in the Supplemental Material [41]).

In the layer-symmetric state the energy is simply given by $E_{\text{sym}}^i(n) = E_{\text{sym}}^{\text{int}}(n)$, where for convenience we set the overall energy reference scale, $E_X^+ = 0$, to zero. By contrast, in the staggered dipolar lattice, in addition to the electrostatic energy, one must also take into account the energy contribution of the quadrupolar to dipolar gap Δ_{DQ} , so that in total $E_{\text{stg}}^i(n) = \Delta_{\text{DQ}} + E_{\text{stg}}^{\text{int}}(n)$. This energy minimization procedure is illustrated in Fig. 2(b), where we depict both E_{sym}^i and E_{stg}^i as a function of n for several pertinent values of R .

We first consider the case of large but finite R . Since Δ_{DQ} and thus R are strictly positive, for sufficiently large R and at low n , where interactions between excitons are negligible, the symmetric quadrupole state ψ_X^+ will always be the lowest energy state, as already discussed above. With an increase of n , the electrostatic energy gain associated with the staggered configuration eventually overwhelms Δ_{DQ} . Therefore, we expect to find a quantum phase transition, at

a critical density $n_c(R)$, where the symmetric quadrupolar state gives way to a staggered dipole configuration. Neglecting quantum fluctuations, the phase transition is expected to be first order in nature (as opposed to the pure Ising universality class), since in addition to breaking of Ising layer symmetry the transition also involves a structural rearrangement, from a triangular to square lattice. The precise phase boundary $n_c(R)$ is determined by carrying out a numerical computation [41].

The above picture is correct for all R values for which $n_c > n_d$. Interestingly, we further identify an additional phase for $R < R_c = R(n_c = n_d) \approx 0.076$. This result follows directly from the nonmonotonous behavior of $E_{\text{stg}}^{\text{int}}(n)$. As is depicted in Fig. 2(b), for any $R < R_c$, there is a density $n_c < n_d$ above which $E_{\text{stg}}^i(n_d) < E_{\text{sym}}^i(n)$. This suggests that a homogeneous symmetric state with a density $n > n_c$ is unstable towards a phase separation and formation of a staggered dipolar droplet with a density n_d . The phase separation consisting of a staggered dipolar droplet is sustained up to $n = n_d$, beyond which the droplet fills the plane and the homogeneous staggered phase is reached. Surprisingly, for $R < 0.036$, $n_c = 0$, and the symmetric quadrupole phase is unstable for any density. Schematic drawing and further analysis of the staggered droplet phase is given in the Supplemental Material [41].

Figure 2(c) presents the general phase diagram of a three-layer system as a function of R and n . Within our approximation, the triple point appears at (n_d, R_c) . Dashed lines represent the predicted possible range of R_{WMW} and thus the possible phases, for the special case of a system of $\text{WSe}_2/\text{MoSe}_2/\text{WSe}_2$ trilayer calculated above. This range results from the uncertainty in calculating both Δ_{WMW} and κ , as discussed above [41]. This clearly demonstrates that such quantum phase transitions are indeed relevant for the TMD trilayer system.

Discussion and summary.—A complete understanding of the low temperature phase diagram of our model will require a refined analysis that takes into account the role of quantum fluctuations and bosonic exchange statistics. These effects may allow access to additional states of matter such as various patterns of exciton condensates and supersolids. Importantly, our many-body Hamiltonian, Eq. (2), is amenable to an exact numerical solution using quantum Monte Carlo techniques. These interesting directions are currently under pursuit.

From the experimental perspective, the symmetric and staggered phases can be identified in optical spectroscopy: (i) By monitoring the changes of the emission or absorption energy with n , controlled by optical excitation power. This way, the theoretically predicted different scaling of $E^i(n)$ of each phase can be traced [see Fig. 2(b) and Fig. S8 in the Supplemental Material [41]], and the phase transition can be detected as a sharp change of the slope of $E^i(n)$. In particular, the droplet phase would be characterized by a regime where the recombination energy is density

independent, and (ii) the radiative rate of quadrupolar excitons is expected to be higher than dipolar excitons due to the larger e - h overlap in the symmetric quadrupolar exciton state [37]. This difference can be utilized to distinguish quadrupolar from dipolar phases, and finally, (iii) the existence of single quadrupolar excitons can be detected as a redshift of $\Delta_{DQ} \sim 30$ meV of the lowest exciton emission line of the trilayer, compared to the bilayer that supports only dipolar excitons. In fact, a comparison between recent experiments on a $\text{WSe}_2/\text{MoSe}_2/\text{WSe}_2$ trilayer [37] with results on a $\text{WSe}_2/\text{MoSe}_2$ bilayer [57], under similar temperature and illumination conditions, shows a 40 meV difference—in good agreement with our predictions.

More generally, our theoretical predictions [Fig. 2(c)] are not unique to the specific $\text{WSe}_2/\text{MoSe}_2/\text{WSe}_2$ heterostructure. In principle, it can be realized in many other trilayer heterostructures of two materials that form a type-II band alignment, and also in three monolayers of the same material separated by insulating spacer layers, with a bias applied between the middle layer and the two lateral layers. Similar potentials can also be designed in semiconductor quantum wells based on, e.g., GaAs and AlAs compounds. In addition, properties such as the dipole length and Δ^\pm , are tunable in each specific structure (by applying an electric gate or pressure). Experiments with different three-layer systems may explore different regimes of the phase diagram.

To summarize, we present a trilayer system as a striking example for the possible rich quantum physics in a system where the single particle properties and the many-body state are no longer separate entities, but rather dynamically coupled through the particle interactions. In the single exciton limit we predict the emergence of a new type of interlayer excitons with a finite electric quadrupole moment. At finite exciton densities, our simple model suggests unique phase transitions that change both the Ising (layer) and lattice symmetries, and the intrinsic nature of each interlayer exciton.

S. R. A. acknowledges support from the Israel Science Foundation, Grant No. 1208/19. S. G. acknowledges support from the Israel Science Foundation, Grant No. 1686/18. R. R. acknowledges support from the Israel Science Foundation, Grant No. 836/17, and the Bi-national Science Foundation, Grant No. 2016112. H. S. acknowledges support from Israeli Science Foundation Grant No. 861/19. This research used resources of the National Energy Research Scientific Computing Center (NERSC).

*Corresponding author.
ronenr@phys.huji.ac.il

- [1] G. E. Astrakharchik, J. Boronat, I. L. Kurbakov, and Y. E. Lozovik, Quantum Phase Transition in a Two-Dimensional System of Dipoles, *Phys. Rev. Lett.* **98**, 060405 (2007).
- [2] H. P. Büchler, E. Demler, M. Lukin, A. Micheli, N. Prokof'ev, G. Pupillo, and P. Zoller, Strongly Correlated 2D Quantum Phases with Cold Polar Molecules: Controlling the Shape of the Interaction Potential, *Phys. Rev. Lett.* **98**, 060404 (2007).
- [3] B. Laikhtman and R. Rapaport, Correlations in a two-dimensional Bose gas with long-range interaction, *Europhys. Lett.* **87**, 27010 (2009).
- [4] L. Chomaz, R. M. W. v. Bijnen, D. Petter, G. Faraoni, S. Baier, J. H. Becher, M. J. Mark, F. Wächtler, L. Santos, and F. Ferlaino, Observation of roton mode population in a dipolar quantum gas, *Nat. Phys.* **14**, 442 (2018).
- [5] L. Tanzi, E. Lucioni, F. Famà, J. Catani, A. Fioretti, C. Gabbanini, R. N. Bisset, L. Santos, and G. Modugno, Observation of a Dipolar Quantum Gas with Metastable Supersolid Properties, *Phys. Rev. Lett.* **122**, 130405 (2019).
- [6] L. Chomaz, D. Petter, P. Ilzhöfer, G. Natale, A. Trautmann, C. Politi, G. Durastante, R. M. W. van Bijnen, A. Patscheider, M. Sohmen, M. J. Mark, and F. Ferlaino, Long-Lived and Transient Supersolid Behaviors in Dipolar Quantum Gases, *Phys. Rev. X* **9**, 021012 (2019).
- [7] F. Böttcher, J.-N. Schmidt, M. Wenzel, J. Hertkorn, M. Guo, T. Langen, and T. Pfau, Transient Supersolid Properties in an Array of Dipolar Quantum Droplets, *Phys. Rev. X* **9**, 011051 (2019).
- [8] M. Guo, F. Böttcher, J. Hertkorn, J.-N. Schmidt, M. Wenzel, H. P. Büchler, T. Langen, and T. Pfau, The low-energy Goldstone mode in a trapped dipolar supersolid, *Nature (London)* **574**, 386 (2019).
- [9] L. Tanzi, S. M. Roccuzzo, E. Lucioni, F. Famà, A. Fioretti, C. Gabbanini, G. Modugno, A. Recati, and S. Stringari, Supersolid symmetry breaking from compressional oscillations in a dipolar quantum gas, *Nature (London)* **574**, 382 (2019).
- [10] G. Natale, R. M. W. van Bijnen, A. Patscheider, D. Petter, M. J. Mark, L. Chomaz, and F. Ferlaino, Excitation Spectrum of a Trapped Dipolar Supersolid and Its Experimental Evidence, *Phys. Rev. Lett.* **123**, 050402 (2019).
- [11] J. P. Eisenstein and A. H. MacDonald, Bose-Einstein condensation of excitons in bilayer electron systems, *Nature (London)* **432**, 691 (2004).
- [12] A. A. High, J. R. Leonard, M. Remeika, L. V. Butov, M. Hanson, and A. C. Gossard, Condensation of excitons in a trap, *Nano Lett.* **12**, 2605 (2012).
- [13] Y. Shilo, K. Cohen, B. Laikhtman, K. West, L. Pfeiffer, and R. Rapaport, Particle correlations and evidence for dark state condensation in a cold dipolar exciton fluid, *Nat. Commun.* **4**, 2335 (2013).
- [14] M. Stern, V. Umansky, and I. Bar-Joseph, Exciton liquid in coupled quantum wells, *Science* **343**, 55 (2014).
- [15] R. Anankine, M. Beian, S. Dang, M. Alloing, E. Cambril, K. Merghem, C. G. Carbonell, A. Lemaître, and F. Dubin, Quantized Vortices and Four-Component Superfluidity of Semiconductor Excitons, *Phys. Rev. Lett.* **118**, 127402 (2017).
- [16] Y. Mazuz-Harpaz, K. Cohen, M. Leveson, K. West, L. Pfeiffer, M. Khodas, and R. Rapaport, Dynamical formation of a strongly correlated dark condensate of dipolar excitons, *Proc. Natl. Acad. Sci. U.S.A.* **116**, 18328 (2019).
- [17] Z. Wang, D. A. Rhodes, K. Watanabe, T. Taniguchi, J. C. Hone, J. Shan, and K. F. Mak, Evidence of high-temperature

- exciton condensation in two-dimensional atomic double layers, *Nature (London)* **574**, 76 (2019).
- [18] L. Sigl, F. Sigger, F. Kronowetter, J. Kiemle, J. Klein, K. Watanabe, T. Taniguchi, J. J. Finley, U. Wurstbauer, and A. W. Holleitner, Condensation signatures of photogenerated interlayer excitons in a van der Waals heterostack, *arXiv:2001.07567*.
 - [19] X. Hong, J. Kim, S.-F. Shi, Y. Zhang, C. Jin, Y. Sun, S. Tongay, J. Wu, Y. Zhang, and F. Wang, Ultrafast charge transfer in atomically thin MoS₂/WS₂ heterostructures, *Nat. Nanotechnol.* **9**, 682 (2014).
 - [20] H. Fang, C. Battaglia, C. Carraro, S. Nemsak, B. Ozdol, J. S. Kang, H. A. Bechtel, S. B. Desai, F. Kronast, A. A. Unal, G. Conti, C. Conlon, G. K. Palsson, M. C. Martin, A. M. Minor, C. S. Fadley, E. Yablonovitch, R. Maboudian, and A. Javey, Strong interlayer coupling in van der Waals heterostructures built from single-layer chalcogenides, *Proc. Natl. Acad. Sci. U.S.A.* **111**, 6198 (2014).
 - [21] P. Rivera, J. R. Schaibley, A. M. Jones, J. S. Ross, S. Wu, G. Aivazian, P. Klement, K. Seyler, G. Clark, N. J. Ghimire, J. Yan, D. G. Mandrus, W. Yao, and X. Xu, Observation of long-lived interlayer excitons in monolayer MoSe₂-WSe₂ heterostructures, *Nat. Commun.* **6**, 6242 (2015).
 - [22] M.-H. Chiu, C. Zhang, H.-W. Shiu, C.-P. Chuu, C.-H. Chen, C.-Y. S. Chang, C.-H. Chen, M.-Y. Chou, C.-K. Shih, and L.-J. Li, Determination of band alignment in the single-layer MoS₂/WSe₂ heterojunction, *Nat. Commun.* **6**, 7666 (2015).
 - [23] A. F. Rigosi, H. M. Hill, Y. Li, A. Chernikov, and T. F. Heinz, Probing interlayer interactions in transition metal dichalcogenide heterostructures by optical spectroscopy: MoS₂/WS₂ and MoSe₂/WSe₂, *Nano Lett.* **15**, 5033 (2015).
 - [24] D. Unuchek, A. Ciarrocchi, A. Avsar, K. Watanabe, T. Taniguchi, and A. Kis, Room-temperature electrical control of exciton flux in a van der Waals heterostructure, *Nature (London)* **560**, 340 (2018).
 - [25] P. Rivera, K. L. Seyler, H. Yu, J. R. Schaibley, J. Yan, D. G. Mandrus, W. Yao, and X. Xu, Valley-polarized exciton dynamics in a 2D semiconductor heterostructure, *Science* **351**, 688 (2016).
 - [26] P. Merkl, F. Mooshammer, P. Steinleitner, A. Girmhuber, K.-Q. Lin, P. Nagler, J. Holler, C. Schüller, J. M. Lupton, T. Korn, S. Ovesen, S. Brem, E. Malic, and R. Huber, Ultrafast transition between exciton phases in van der Waals heterostructures, *Nat. Mater.* **18**, 691 (2019).
 - [27] Y. Tang, L. Li, T. Li, Y. Xu, S. Liu, K. Barmak, K. Watanabe, T. Taniguchi, A. H. MacDonald, J. Shan, and K. F. Mak, Simulation of Hubbard model physics in WSe₂/WS₂ moiré superlattices, *Nature (London)* **579**, 353 (2020).
 - [28] Y. Shimazaki, I. Schwartz, K. Watanabe, T. Taniguchi, M. Kroner, and A. Imamoğlu, Strongly correlated electrons and hybrid excitons in a moiré heterostructure, *Nature (London)* **580**, 472 (2020).
 - [29] C. Jin, E. Y. Ma, O. Karni, E. C. Regan, F. Wang, and T. F. Heinz, Ultrafast dynamics in van der Waals heterostructures, *Nat. Nanotechnol.* **13**, 994 (2018).
 - [30] L. A. Jauregui, A. Y. Joe, K. Pistunova, D. S. Wild, A. A. High, Y. Zhou, G. Scuri, K. De Greve, A. Sushko, C.-H. Yu, T. Taniguchi, K. Watanabe, D. J. Needleman, M. D. Lukin, H. Park, and P. Kim, Electrical control of interlayer exciton dynamics in atomically thin heterostructures, *Science* **366**, 870 (2019).
 - [31] A. Ciarrocchi, D. Unuchek, A. Avsar, K. Watanabe, T. Taniguchi, and A. Kis, Polarization switching and electrical control of interlayer excitons in two-dimensional van der Waals heterostructures, *Nat. Photonics* **13**, 131 (2019).
 - [32] R. Gillen and J. Maultzsch, Interlayer excitons in MoS₂/WSe₂ heterostructures from first principles, *Phys. Rev. B* **97**, 165306 (2018).
 - [33] E. Torun, H. P. C. Miranda, A. Molina-Sánchez, and L. Wirtz, Interlayer and intralayer excitons in MoS₂/WS₂ and MoSe₂/WSe₂ heterobilayers, *Phys. Rev. B* **97**, 245427 (2018).
 - [34] S. Ovesen, S. Brem, C. Linderålv, M. Kuisma, T. Korn, P. Erhart, M. Selig, and E. Malic, Interlayer exciton dynamics in van der Waals heterostructures, *Commun. Phys.* **2**, 23 (2019).
 - [35] E. Y. Paik, L. Zhang, G. W. Burg, R. Gogna, E. Tutuc, and H. Deng, Interlayer exciton laser of extended spatial coherence in atomically thin heterostructures, *Nature (London)* **576**, 80 (2019).
 - [36] M. Baranowski, A. Surrente, L. Kłopotowski, J. M. Urban, N. Zhang, D. K. Maude, K. Wiwatowski, S. Mackowski, Y. C. Kung, D. Dumcenco, A. Kis, and P. Plochocka, Probing the inter-layer exciton physics in a MoS₂/MoSe₂/MoS₂ van der Waals heterostructure, *Nano Lett.* **17**, 6360 (2017).
 - [37] C. Choi, J. Huang, H.-C. Cheng, H. Kim, A. K. Vinod, S.-H. Bae, V. O. Özçelik, R. Grassi, J. Chae, S.-W. Huang, X. Duan, K. Kaasbjerg, T. Low, and C. W. Wong, Enhanced interlayer neutral excitons and trions in trilayer van der Waals heterostructures, *npj 2D Mater. Appl.* **2**, 1 (2018).
 - [38] M. S. Hybertsen and S. G. Louie, First-Principles Theory of Quasiparticles: Calculation of Band Gaps in Semiconductors and Insulators, *Phys. Rev. Lett.* **55**, 1418 (1985).
 - [39] M. Rohlfing and S. G. Louie, Electron-hole excitations and optical spectra from first principles, *Phys. Rev. B* **62**, 4927 (2000).
 - [40] J. Deslippe, G. Samsonidze, D. A. Strubbe, M. Jain, M. L. Cohen, and S. G. Louie, BerkeleyGW: A massively parallel computer package for the calculation of the quasiparticle and optical properties of materials and nanostructures, *Comput. Phys. Commun.* **183**, 1269 (2012).
 - [41] See Supplemental Material at <http://link.aps.org/supplemental/10.1103/PhysRevLett.125.255301> for further discussion and analysis of the different phases, as well as technical details regarding all calculations, which includes Refs. [42–55].
 - [42] W. Kohn and L. J. Sham, Self-consistent equations including exchange and correlation effects, *Phys. Rev.* **140**, A1133 (1965).
 - [43] P. Giannozzi *et al.*, Advanced capabilities for materials modelling with quantum espresso, *J. Phys. Condens. Matter* **29**, 465901 (2017).
 - [44] V. R. Cooper, Van der Waals density functional: An appropriate exchange functional, *Phys. Rev. B* **81**, 161104(R) (2010).
 - [45] M. Dion, H. Rydberg, E. Schröder, D. C. Langreth, and B. I. Lundqvist, Van der Waals Density Functional for General Geometries, *Phys. Rev. Lett.* **92**, 246401 (2004).
 - [46] J. P. Perdew, K. Burke, and M. Ernzerhof, Generalized Gradient Approximation made Simple, *Phys. Rev. Lett.* **77**, 3865 (1996).

- [47] S. Grimme, J. Antony, S. Ehrlich, and H. Krieg, A consistent and accurate ab initio parametrization of density functional dispersion correction (DFT-D) for the 94 elements H-Pu, *J. Chem. Phys.* **132**, 154104 (2010).
- [48] F. H. da Jornada, D. Y. Qiu, and S. G. Louie, Nonuniform sampling schemes of the brillouin zone for many-electron perturbation-theory calculations in reduced dimensionality, *Phys. Rev. B* **95**, 035109 (2017).
- [49] S. Ismail-Beigi, Truncation of periodic image interactions for confined systems, *Phys. Rev. B* **73**, 233103 (2006).
- [50] D. Y. Qiu, F. H. da Jornada, and S. G. Louie, Optical Spectrum of MoS₂: Many-Body Effects and Diversity of Exciton States, *Phys. Rev. Lett.* **111**, 216805 (2013).
- [51] D. Y. Qiu, F. H. da Jornada, and S. G. Louie, Screening and many-body effects in two-dimensional crystals: Monolayer MoS₂, *Phys. Rev. B* **93**, 235435 (2016).
- [52] G. H. Wannier, Antiferromagnetism. The triangular Ising net, *Phys. Rev.* **79**, 357 (1950).
- [53] D. R. Nelson, *Defects and Geometry in Condensed Matter Physics* (Cambridge University Press, Cambridge, England, 2002).
- [54] H. R. Glyde, *Excitations in Liquid and Solid Helium* (Clarendon Press, Oxford, 1994).
- [55] R. Rapaport and G. Chen, Experimental methods and analysis of cold and dense dipolar exciton fluids, *J. Phys. Condens. Matter* **19**, 295207 (2007).
- [56] M. Sammon and B. I. Shklovskii, Attraction of indirect excitons in van der Waals heterostructures with three semiconducting layers, *Phys. Rev. B* **99**, 165403 (2019).
- [57] B. Miller, A. Steinhoff, B. Pano, J. Klein, F. Jahnke, A. Holleitner, and U. Wurstbauer, Long-lived direct and indirect interlayer excitons in van der Waals heterostructures, *Nano Lett.* **17**, 5229 (2017).